

Probing the Effective Quantum Gravity via Quasinormal Modes and Shadows of Black Holes

R. A. Konoplya^{1,*} and O. S. Stashko^{2,†}

¹*Research Centre for Theoretical Physics and Astrophysics,
Institute of Physics, Silesian University in Opava,
Bezručovo náměstí 13, CZ-74601 Opava, Czech Republic*

²*Princeton University, Princeton, NJ, 08544, USA*

Two quantum-corrected black hole models have recently been proposed within the Hamiltonian constraints approach to quantum gravity, maintaining general covariance [1]. We have studied the quasinormal spectra of these black holes using four methods: the higher-order WKB approach with Padé approximants, time-domain integration, Frobenius, and pseudospectral methods. The Frobenius method, in particular, allows us to determine precise values of the frequencies, including the overtones. The two models differ in their choice of quantum parameter ξ , and we can distinguish them by their quasinormal spectra. In the first model, increasing the quantum parameter results in higher real oscillation frequencies and damping rates of the fundamental mode. In contrast, the second model shows a decrease in the oscillation frequency of the least-damped mode when the quantum parameter is introduced. We have shown that, while the fundamental mode changes relatively gradually with the quantum parameter, the first few overtones deviate from their Schwarzschild limits at an increasing rate. This results in a qualitatively new behavior: the real parts of the frequencies of the first and higher overtones tend to zero as the quantum parameter increases. In addition to the branch of modes that are perturbative in the quantum parameter, we observe some non-perturbative modes at moderate values of the quantum parameter. Additionally, we have calculated the radii of the shadows cast by these black holes and discussed possible constraints based on observations of Sgr A*.

I. INTRODUCTION

Efforts to find quantum corrections to the black hole metric involve various theoretical frameworks aimed at integrating quantum field theory with general relativity. Loop Quantum Gravity (LQG) modifies spacetime near singularities, providing non-singular black hole solutions [2]. String theory introduces higher-order curvature corrections and interprets black hole entropy through microstates [3]. Effective Field Theory (EFT) approaches add higher-derivative terms to the gravitational action, leading to modified metrics [4]. Non-commutative geometry proposes a fundamental length scale, smoothing out singularities [5]. The AdS/CFT correspondence translates quantum corrections from conformal field theory to modifications in the AdS black hole metric [6]. Lastly, the asymptotic safety program uses renormalization group flow to derive consistent high-energy black hole solutions [7].

A particular approach to quantum corrections for the black hole spacetime we are interested about is related to the Hamiltonian constraints approach [8, 9]. The Hamiltonian constraints approach is a significant method in the quest for quantum gravity, particularly in the canonical quantization of general relativity. This approach involves reformulating Einstein's equations in terms of a Hamiltonian framework, where the dynamics of the gravitational

field are governed by constraints. These constraints ensure the preservation of general covariance, meaning that the physical predictions do not depend on the choice of coordinates. In the context of black holes, the Hamiltonian constraints approach allows for the inclusion of quantum corrections by modifying the Hamiltonian to incorporate quantum effects.

Recently, a long-standing issue regarding general covariance in spherically symmetric gravity, which arises when canonical quantum gravity leads to a semiclassical model of black holes, was addressed in [1]. This work proposed two black hole models that differ based on the choice of a quantum parameter.

The fundamental characteristic of black hole geometry is its spectrum of quasinormal modes [10, 11], which can be observed through gravitational wave interferometers [12, 13]. Future experiments promise to detect a much broader range of frequencies [14]. While the fundamental mode primarily depends on the peak of the potential barrier, the first few overtones describe the geometry near the event horizon [15, 16]. In the time domain, these first overtones are crucial for describing the initial stage of the ringdown [17]. Observations in the gravitational spectrum can be complemented by electromagnetic observations, such as measuring the shadows cast by black holes [18] and analyzing other optical phenomena [19].

While numerous studies have explored quasinormal modes of quantum-corrected black holes [20–32], the recent models produced within the effective Hamiltonian approach, maintaining general covariance, as presented in [1], have not been previously considered.

In this study, we investigate the quasinormal frequen-

* roman.konoplya@gmail.com

† alexander.stashko@gmail.com

cies of the two black hole metrics derived in [1] for scalar, electromagnetic, and effective axial gravitational perturbations. We employ four independent methods for these calculations: the higher-order WKB approach with Padé approximants, time-domain integration, the Frobenius method and the pseudospectral method. The Frobenius method, in particular, provides precise results, enabling us to determine accurate values for the overtones. Our findings reveal that while the fundamental mode changes relatively mildly upon the introduction of quantum corrections, the first few overtones deviate significantly, with their real oscillation frequencies tending towards zero. This behavior creates a distinctive "sound" of the event horizon deformed by quantum corrections. When the quantum parameter is not sufficiently small, we observe quasinormal modes that do not transition into the Schwarzschild modes as the quantum parameter approaches zero. In addition, we calculate the radius of the shadow cast by these two black holes.

The structure of our work is as follows. In Section II, we introduce the black hole metrics and discuss the wave equations for scalar, electromagnetic, and effective gravitational perturbations. Section III reviews the four methods used for calculating the quasinormal frequencies. In Section IV, we present the numerical results for the quasinormal modes and provide analytical solutions in the eikonal regime. Section V is devoted to the discussion of the shadows cast by these black holes. Finally, in the Conclusions, we discuss our findings and highlight some open problems.

II. BLACK HOLE METRIC AND WAVE-LIKE EQUATIONS

A. The metric and the underlying theory

The work of [1] addresses the issue of maintaining covariance within the context of the spherically symmetric sector of vacuum gravity. By retaining the theory's kinematical variables and the classical form of the vector constraints, the study introduces an arbitrary effective Hamiltonian constraint, H_{eff} , along with a freely chosen function in constructing the effective metric. It is assumed, as in the classical theory, that a Dirac observable representing the black hole mass exists. Given these assumptions, the authors establish conditions on this observable and derive equations that ensure space-time covariance. These conditions lead to relationships between the effective Hamiltonian, the Dirac observable for the black hole mass, and the free function. Solving these equations yields two families of effective Hamiltonian constraints, each parameterized by its own quantum parameter. Setting these parameters to zero recovers the classical constraints. Consequently, these effective Hamiltonian constraints produce two distinct quantum-corrected metrics, resulting in different spacetime structures.

The metric of the quantum-corrected black hole is given by the following line element

$$ds^2 = -f(r)dt^2 + \frac{1}{g(r)}dr^2 + r^2(d\theta^2 + \sin^2\theta d\phi^2), \quad (1)$$

where for the first type black-hole model, the metric functions are

$$\begin{aligned} f(r) &= \left(1 - \frac{2M}{r}\right) \left[1 + \frac{\xi^2}{r^2} \left(1 - \frac{2M}{r}\right)\right], \\ g(r) &= f(r). \end{aligned}$$

Here ξ is the quantum parameter, and M is the ADM mass.

For the second black hole model, we have:

$$\begin{aligned} f(r) &= 1 - \frac{2M}{r}, \\ g(r) &= f(r) \left(1 + \frac{\xi^2}{r^2} f(r)\right). \end{aligned}$$

The advantage of this black hole metric is that it maintains the same relationship between the event horizon radius r_h^+ and the black hole mass as the classical solution, $r_h^+ = 2M$. This consistency facilitates an easy comparison between the spectra of classical and quantum-corrected black holes.

B. Perturbation of test fields

The general relativistic equations for the scalar (Φ) and electromagnetic (A_μ), can be written in the following form:

$$\frac{1}{\sqrt{-g}}\partial_\mu(\sqrt{-g}g^{\mu\nu}\partial_\nu\Phi) = 0, \quad (2a)$$

$$\frac{1}{\sqrt{-g}}\partial_\mu(F_{\rho\sigma}g^{\rho\nu}g^{\sigma\mu}\sqrt{-g}) = 0, \quad (2b)$$

where $F_{\mu\nu} = \partial_\mu A_\nu - \partial_\nu A_\mu$ is the electromagnetic tensor.

After separation of the variables in the background (1) the above equations (2) take the Schrödinger wavelike form [10, 11, 33]:

$$\frac{d^2\Psi}{dr_*^2} + (\omega^2 - V(r))\Psi = 0, \quad (3)$$

where the "tortoise coordinate" r_* is defined as follows:

$$dr_* \equiv \frac{dr}{\sqrt{f(r)g(r)}}. \quad (4)$$

The effective potentials for the scalar ($s = 0$) and electromagnetic ($s = 1$) fields have the form

$$V(r) = f(r) \frac{\ell(\ell+1)}{r^2} + \frac{1-s}{r} \cdot \frac{d^2r}{dr_*^2}, \quad (5)$$

where $\ell = s, s+1, s+2, \dots$ are the multipole numbers.

The effective potentials for the above fields are shown in figs. 1-3. They are positive definite, which guarantees stability for these perturbations.

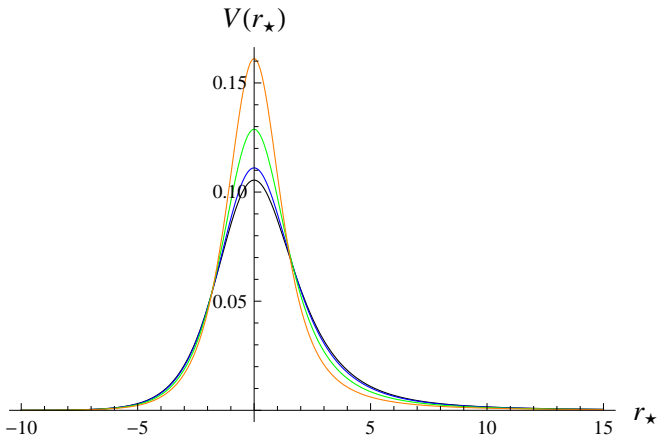


FIG. 1. Effective potential as a function of the tortoise coordinate of the $\ell = 0$ scalar field perturbations of the first black hole model ($M = 1/2$): $\xi = 0$ (black), $\xi = 0.4$ (blue), $\xi = 0.8$ (green), $\xi = 1.2$ (orange).

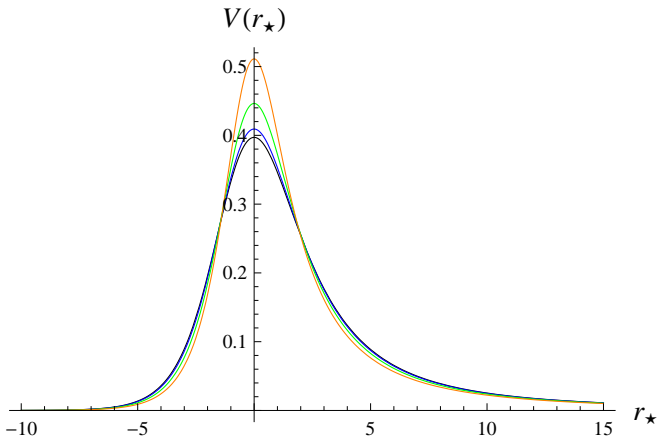


FIG. 2. Effective potential as a function of the tortoise coordinate of the $\ell = 1$ scalar field perturbations of the first black hole model ($M = 1/2$): $\xi = 0$ (black), $\xi = 0.4$ (blue), $\xi = 0.8$ (green), $\xi = 1.2$ (orange).

C. Perturbations of gravitational field

The problem of gravitational perturbations is more complex in this case because the metric is derived through an effective approach using Hamiltonian constraints, rather than being an exact solution of the Einstein equations with quantum corrections. Consequently, a rigorous analysis of gravitational perturbations is challenging to achieve. However, as demonstrated by Ashtekar, Olmedo, and Singh [34, 35], quantum corrections can be effectively modeled as contributions from an anisotropic fluid's energy-momentum tensor within the framework of Einsteinian gravity. This allows for the study of perturbations in such a system. Following the

work of Bouhmadi-López et al. [36], axial perturbations can be analyzed under the assumption that perturbations in the direction of the anisotropy are negligible in

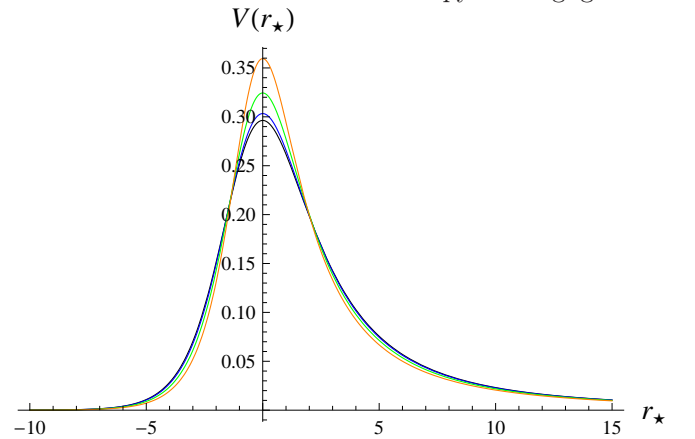


FIG. 3. Effective potential as a function of the tortoise coordinate of the $\ell = 1$ electromagnetic field perturbations of the first black hole model ($M = 1/2$): $\xi = 0$ (black), $\xi = 0.4$ (blue), $\xi = 0.8$ (green), $\xi = 1.2$ (orange).

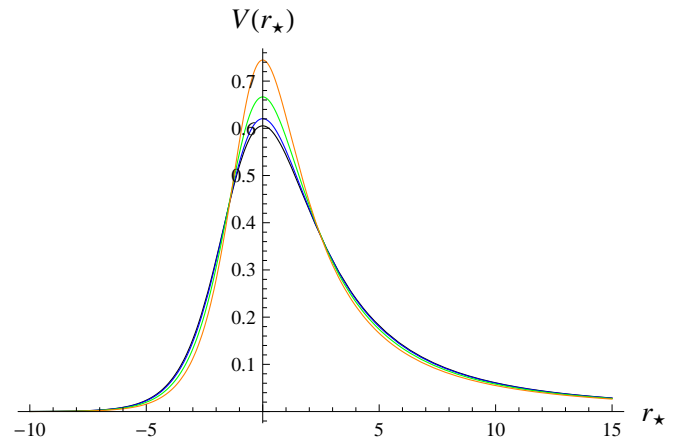


FIG. 4. Effective potential as a function of the tortoise coordinate of the $\ell = 2$ axial gravitational perturbations of the first black hole model ($M = 1/2$): $\xi = 0$ (black), $\xi = 0.4$ (blue), $\xi = 0.8$ (green), $\xi = 1.2$ (orange).

the axial sector of gravitational perturbations.

There are several similar instances where certain perturbations are considered relatively minor and thus neglected [37–39]. While this approach may overlook some significant features of the gravitational spectrum, it serves as a reasonable approximation, especially when the black hole geometry deviates only slightly from the classical Schwarzschild limit. This approximation aligns with the concept of perturbative quantum corrections, which are expected to be relatively small.

The metrics of the axial gravitational perturbations $h_{\mu\nu}$ in the Regge-Wheeler gauge [40] take the following form

$$h_{\mu\nu}^{axial} = \begin{bmatrix} 0 & 0 & 0 & h_0(t, r) \\ 0 & 0 & 0 & h_1(t, r) \\ 0 & 0 & 0 & 0 \\ h_0(t, r) & h_1(t, r) & 0 & 0 \end{bmatrix} \left(\sin\theta \frac{\partial}{\partial\theta} \right) P_\ell(\cos\theta), \quad (6)$$

where $h_0(t, r)$ and $h_1(t, r)$ are two unknown functions, and $P_\ell(x)$ is the Legendre polynomial.

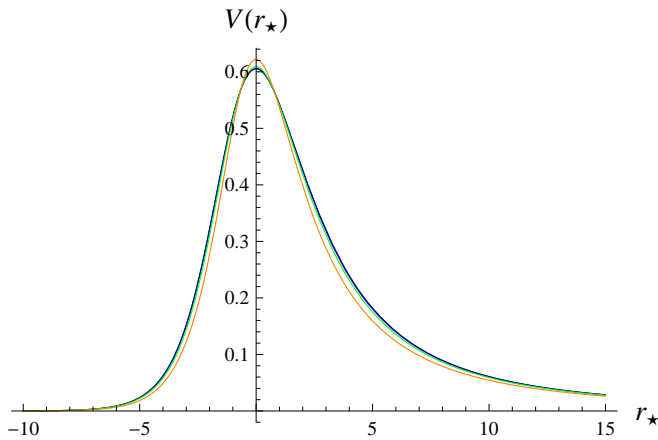


FIG. 5. Effective potential as a function of the tortoise coordinate of the $\ell = 2$ axial gravitational perturbations of the second black hole model ($M = 1/2$): $\xi = 0$ (black), $\xi = 0.4$ (blue), $\xi = 0.8$ (green), $\xi = 1.6$ (orange).

The solutions can be considered as solutions of the Einstein equations with some anisotropic fluid with

$$T_{\mu\nu} = (\rho + p_t)u_{\mu\nu} + g_{\mu\nu}p_t + (p_r - p_t)s_\mu s_\nu, \quad (7)$$

where ρ , p_r , p_t are the fluid density, radial, and tangential pressure, respectively. The fluid velocity u_μ , and radial space-like unit vector s_μ , are given by

$$u_\mu = (\sqrt{f(r)}, 0, 0, 0), \quad s_\mu = (0, 1/\sqrt{g(r)}, 0, 0). \quad (8)$$

They satisfy

$$u_\mu u^\mu = -1, \quad s_\mu s^\mu = 1, \quad u_\mu s^\mu = 0. \quad (9)$$

The quantities ρ , p_r , p_t transform as scalars relatively the rotation group on the two dimensional sphere, so their axial perturbations are zero. For u_μ and s_μ vectors we have nonzero perturbations components

$$\delta u_\phi = -i\omega U(r)e^{-i\omega t} \sin\theta \partial_\theta P_\ell(\cos\theta) \quad (10)$$

$$\delta s_\phi = -S(r)e^{-i\omega t} \sin\theta \partial_\theta P_\ell(\cos\theta), \quad (11)$$

Further, we assume that there are no perturbations in the anisotropy direction, i.e. $\delta s_\mu = 0$.

From $\nabla_\mu T^{\mu r} = 0$, we obtain that $\delta u_\phi = 0$. After substitution into the Einstein equations we obtain

$$h_1(r) (r^2\omega^2 - (\ell-1)(\ell+2)f(r)) - ir^2\omega h_0'(r) + 2ir\omega h_0(r) = 0, \quad (12)$$

$$f(r) \left(\frac{h_1(r)f'(r)}{f(r)} + 2h_1'(r) \right) + \frac{2i\omega h_0(r)}{g(r)} = 0, \quad (13)$$

After simple algebra and introducing new variables

$$h_1 = \frac{r}{\sqrt{f(r)g(r)}}\Psi, \quad dr_* = \frac{dr}{\sqrt{f(r)g(r)}}, \quad (14)$$

we obtain

$$\frac{d^2}{dr_*^2}\Psi + [\omega^2 - V_{ax}(r)] = 0, \quad (15)$$

$$V_{ax} = f(r) \left(\frac{2g(r)}{r^2} - \frac{(fg)'}{2rf} + \frac{(\ell+2)(\ell-1)}{r^2} \right). \quad (16)$$

A similar approach was used in [41] for studying perturbations of a black hole spacetime with a scalar field, where the scalar field perturbations decouple from the axial gravitational perturbations (see also [42]).

The effective potential for axial gravitational perturbations is shown in figs. 4 and 5. There one can see that the effective potentials are positive definite, which guarantees the stability of the black hole model at least within the framework of the considered effective types of perturbations.

III. METHODS

Here we briefly review the four methods used for the calculations of quasinormal modes: the WKB method, time-domain integration, the Frobenius method, and the pseudospectral method. The Frobenius method is based on a converging procedure and, therefore, provides precise values of quasinormal frequencies.

By definition, quasinormal modes satisfy the following boundary conditions,

$$\Psi(r_* \rightarrow \pm\infty) \propto e^{\pm i\omega r_*}, \quad (17)$$

which are requirement of the purely ingoing waves at the event horizon ($r_* \rightarrow -\infty$) and purely outgoing wave at spatial infinity ($r_* \rightarrow \infty$).

A. WKB method

The WKB approach is an effective and apparently the most economic way to find quasinormal modes with $\ell \geq n$. It consists of matching of the asymptotic WKB

solutions with the Taylor expansion of the wave function around the maximum of the potential barrier. The general WKB formula can be written in the form of expansion around the eikonal limit ($\ell \gg n$) [43]:

$$\omega^2 = V_0 + A_2(\mathcal{K}^2) + A_4(\mathcal{K}^2) + A_6(\mathcal{K}^2) + \dots \quad (18)$$

$$- i\mathcal{K}\sqrt{-2V_2} (1 + A_3(\mathcal{K}^2) + A_5(\mathcal{K}^2) + A_7(\mathcal{K}^2) \dots),$$

and the matching conditions under the assumptions of the quasinormal modes boundary conditions produce

$$\mathcal{K} = n + \frac{1}{2}, \quad n = 0, 1, 2, \dots, \quad (19)$$

where n is the overtone number, and V_i is the value of the i -th derivative of effective potential at its maximum relatively the tortoise coordinate. The functions A_i for $i = 2, 3, 4, \dots$ are i -th WKB order correction terms to the eikonal limit, which depends on \mathcal{K} and derivatives of the potential in its maximum up to the order $2i$. The explicit forms of A_i at various i can be found in [44–47]. In the present paper we used the 6th order WKB method [45] with Pade approximants [47]. For the Pade approximants we used $\tilde{m} = 4$ as defined in [43].

B. Time-domain integration

Using integration in the time domain at a fixed value of the radial coordinate, one can see the evolution of the wave function. For such integration we use the Gundlach-Price-Pullin discretization scheme [48]

$$\Psi(N) = \Psi(W) + \Psi(E) - \Psi(S)$$

$$- \Delta^2 V(S) \frac{\Psi(W) + \Psi(E)}{4} + \mathcal{O}(\Delta^4), \quad (20)$$

where the points are defined as follows: $N \equiv (u + \Delta, v + \Delta)$, $W \equiv (u + \Delta, v)$, $E \equiv (u, v + \Delta)$, and $S \equiv (u, v)$.

Then, in order to extract the values of frequencies from the time-domain profile, we use the Prony method, which consists in fitting of the profile data by a sum of exponents with some weights:

$$\Psi(t) \simeq \sum_{i=1}^p C_i e^{-i\omega_i t}. \quad (21)$$

Then, assuming that the ringing starts at some time, we can find the quasinormal frequencies.

C. Frobenius method

The Frobenius method for solutions of differential equations has been well-known for a long time and was applied for the first time by Leaver [49, 50] to the problem of finding of quasinormal modes of black holes. The method is based on expansion into converging series and

therefore it gives the frequencies with any desired precision. For quicker convergence we use the Nollert technique [51] in its general form developed in [52].

The wave-like equation has regular singular points at $r = 0$, at the inner and outer horizons $r = r_h^-$, $r = r_h^+$, and an irregular singular point at $r = \infty$. We introduce a new radial function $P(r, \omega)$,

$$\Psi(r) = P(r, \omega)y(r), \quad (22)$$

such that the factor $P(r, \omega)$ makes $y(r)$ regular in the range $r_h^+ \leq r$ when the quasinormal modes boundary conditions are satisfied. Then, expanding $y(r)$ as follows

$$y(r) = \sum_{k=0}^{\infty} a_k \left(\frac{r - r_h^+}{r - r_h^-} \right)^k, \quad (23)$$

with

$$P(r, \omega) = \left(\frac{r - r_h^+}{r - r_h^-} \right)^{-\frac{i\omega}{f'(r_h^+)}} (r - r_h^-)^{2ir_h^+\omega} e^{i\omega r}, \quad (24)$$

and using Gaussian eliminations, we reduce finding of ω to the problem of numerical solution of a non-algebraic equation via the FindRoot command in *Mathematica*. If even after the above procedure for a chosen $P(r, \omega)$ at some ω , the singular points appear between the event horizon and infinity, we use integration through a sequence of positive real midpoints as suggested by [53].

D. Pseudospectral method

The Chebyshev pseudospectral method is a powerful technique for solving differential equations. The method is based on discretizing the unknown function over a grid of collocation points, typically corresponding to the roots of Chebyshev polynomials. By transforming the differential equations into a system of algebraic equations at these collocation points and solving them, we can determine the function's values at grid points.

To ensure the correct boundary conditions corresponding to quasinormal modes, we make a substitution in the master equation (3)

$$\Psi(r) = r^{2ir_h^+\omega} (r - r_h^+)^{-ir_h^+\omega} e^{i\omega r} y(r), \quad (25)$$

which leads to $y \sim const$ at the outer black hole horizon and at spatial infinity.

Then, we compactify our semi-interval $[r_h, \infty)$ to interval $[0, 1]$ by introducing a new variable

$$r = \frac{r_h}{1 - u}, \quad (26)$$

Altogether, these substitutions lead to an equation of the form

$$A_2(u)y''(u) + A_1(u)y'(u) + A_0(u)y(u) = 0, \quad (27)$$

where $A_i(u) = A_i(u, \omega, \omega^2)$, $i = 0, 1, 2$. At the next step, we discretize equation (27) on the Chebyshev-Lobatto grid, which is defined as

$$u_j = \frac{1}{2} \left(1 - \cos \left[\frac{\pi j}{N} \right] \right), \quad j = 0, 1, \dots, N. \quad (28)$$

This results in a matrix equation

$$\left(\tilde{M}_0 + \tilde{M}_1 \omega + \tilde{M}_2 \omega^2 \right) \tilde{y} = 0, \quad (29)$$

where \tilde{y} is the vector of the unknown function's values, \tilde{M}_i are the numerical matrices of discretized coefficients at the collocation grid points.

We can linearize our quadratic eigenproblem (29) in the following way

$$(M_0 + M_1 \omega) \tilde{\psi} = 0, \quad (30)$$

where

$$M_0 = \begin{pmatrix} \tilde{M}_0 & \tilde{M}_1 \\ 0 & \mathbb{1} \end{pmatrix}, \quad M_1 = \begin{pmatrix} 0 & \tilde{M}_2 \\ -\mathbb{1} & 0 \end{pmatrix}, \quad \tilde{\psi} = \begin{pmatrix} \tilde{y} \\ \omega \tilde{y} \end{pmatrix}. \quad (31)$$

Then QNMs spectrum can be found by solving generalized eigenvalue problem (30) via the Eigenvalues command in *Mathematica*. To avoid spurious eigenvalues we perform the calculations on two grids of different sizes and select only overlapping values [54].

IV. QUASINORMAL MODES

An important preliminary question is determining the range of the quantum correction parameter ξ within which to calculate the quasinormal modes. Since ξ is derived via a perturbative approach, it is not expected to be large. Our criterion for the upper limit is straightforward: if increasing ξ leads to significant changes in the geometry, such that gauge-invariant characteristics, like the fundamental quasinormal mode or the rotational frequency at the innermost stable circular orbit, exhibit more than relatively minor corrections (e.g., several or at most a few tens of percent), then we consider the deviation from the Schwarzschild geometry too strong. At such a point, higher-order corrections should be considered. This criterion guided our choice of the range for ξ , which was kept below 1.4 in most cases.

The fundamental quasinormal modes for both black hole models are presented in Tables I-VIII. A notable difference between the modes of the first and second models is observed in the real oscillation frequency. For the second model, this frequency changes very slightly as the parameter ξ is introduced, whereas it increases with ξ in the first model. This behavior can be attributed to the differences in the black hole metrics: in the first model, both the components g_{tt} and g_{rr} differ from the Schwarzschild case, while in the second model, g_{tt} retains the Schwarzschild form. As a result, the real part of the

frequency, $\text{Re}(\omega)$, which is primarily determined by the centrifugal part of the effective potential, exhibits only minor changes with ξ .

It can be observed that the real oscillation frequency of the fundamental mode increases monotonically with the parameter ξ for perturbations of all types of the first model and for scalar perturbations of the second model. However, this is not the case of the electromagnetic and gravitational perturbations of the second black hole model. Such behavior could be explained by the form of the effective potentials which are higher for larger values of ξ (see figs. 1-4), while this is not so for the perturbations of the second model, as can be seen directly from the analytic expression for the potential fig. 5. The damping rate also generally increases with ξ , up to a certain relatively large value, beyond which it may start to decrease, as illustrated in Fig. 7. A comparison of the WKB approach, time-domain integration, and the precise results of the Frobenius method indicates that while the WKB method can be more accurate for $\ell = 0$, the time-domain integration becomes more reliable for larger values of ℓ . This difference in accuracy arises because, at $\ell = 0$, the ringing period is very short, making it challenging for the Prony method to extract frequencies with high precision.

The most striking effect is not observed in the fundamental mode, which changes relatively smoothly with the parameter ξ , but rather in the first few overtones, which deviate from their Schwarzschild values at an increasing rate. As depicted in the figures, while the fundamental mode only changes by a few percent, the first overtone can change by orders of magnitude. Moreover, we observe a qualitative change in the spectrum of overtones, as the real part of the frequency, $\text{Re}(\omega)$, tends to zero. A similar phenomenon of the vanishing real oscillation frequency of the overtones in the presence of quantum corrections was recently observed in [55]. This vanishing real part of the frequency can also occur for massive fields [56, 57].

The observed high sensitivity of the overtones compared to the fundamental mode can be explained as follows: while the fundamental mode is primarily determined by the behavior of the effective potential near the peak of the potential barrier and is relatively insensitive to near-horizon deformations, the overtones are highly sensitive even to slight near-horizon deformations [15, 16]. This phenomenon, which can be thought of as the "sound" of the event horizon, has been termed the "outburst of overtones" and has recently been the subject of several studies [20, 58–62]. It is interesting to note that, with respect to the behavior of overtones, the two models also exhibit differences: the deviations of overtones from their Schwarzschild values for gravitational perturbations develop much more slowly in the second black hole model than in the first one.

In addition to the quasinormal modes described above, which transition into the Schwarzschild modes as the quantum parameter approaches zero, we observe some

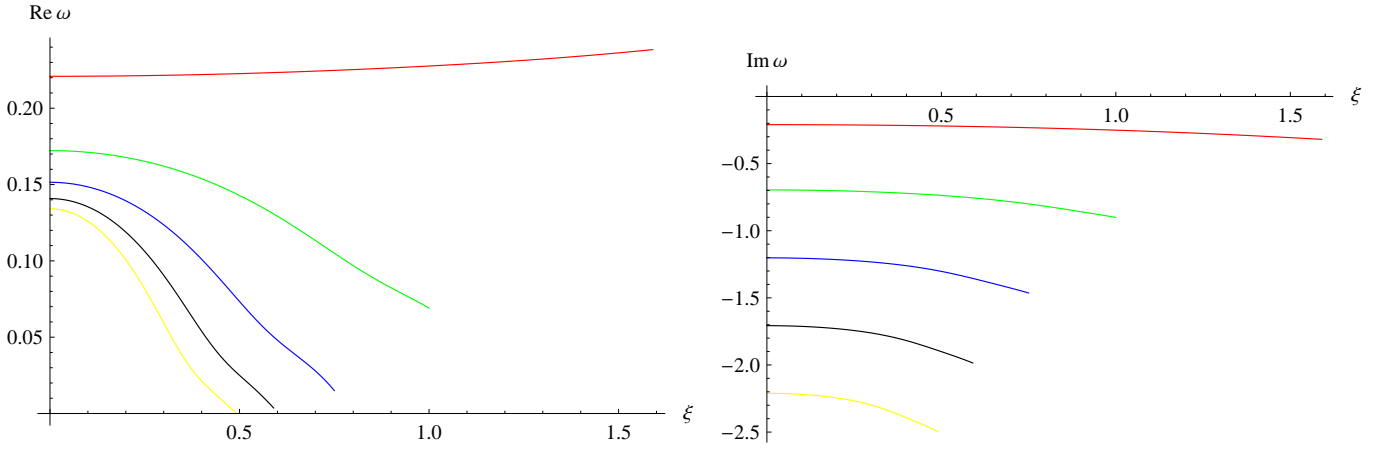


FIG. 6. The fundamental mode and the first four overtones as a function of ξ for the first black-hole model; $\ell = 0$ scalar field perturbations.

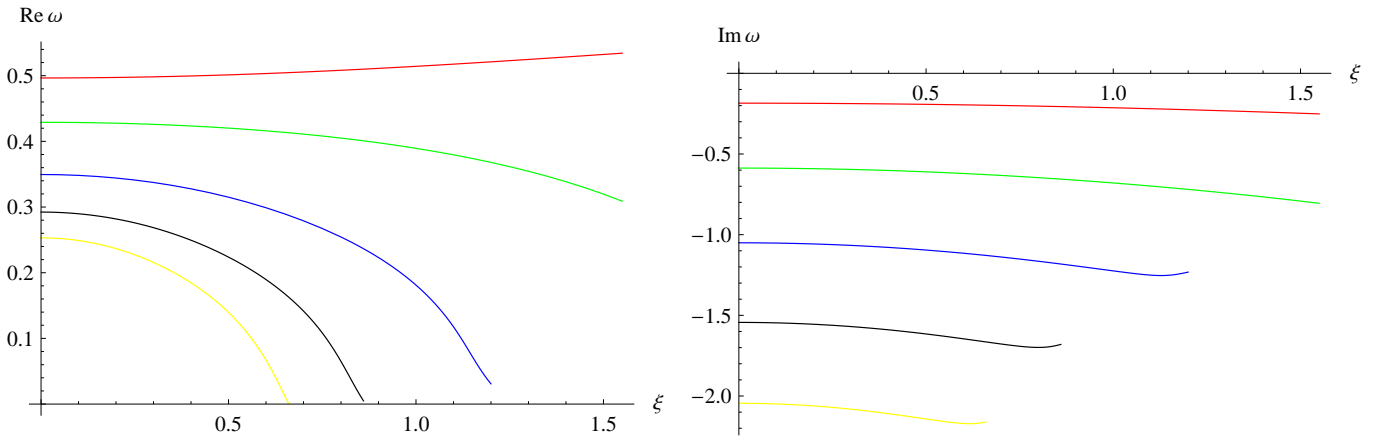


FIG. 7. The fundamental mode and the first four overtones as a function of ξ for the first black-hole model; $\ell = 1$ electromagnetic field perturbations.

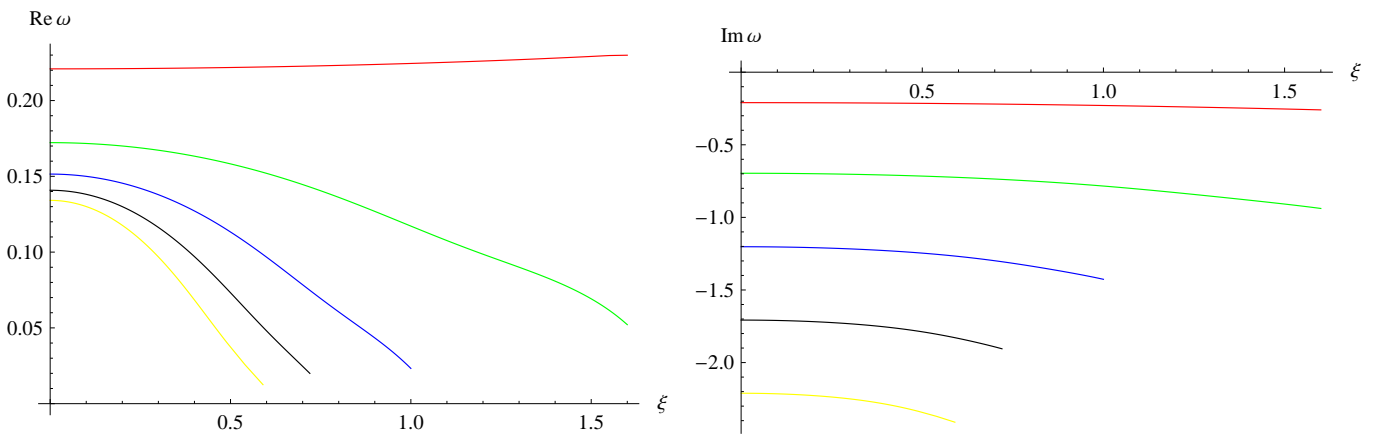


FIG. 8. The fundamental mode and the first four overtones as a function of ξ for the second black-hole model; $\ell = 0$ scalar field perturbations.

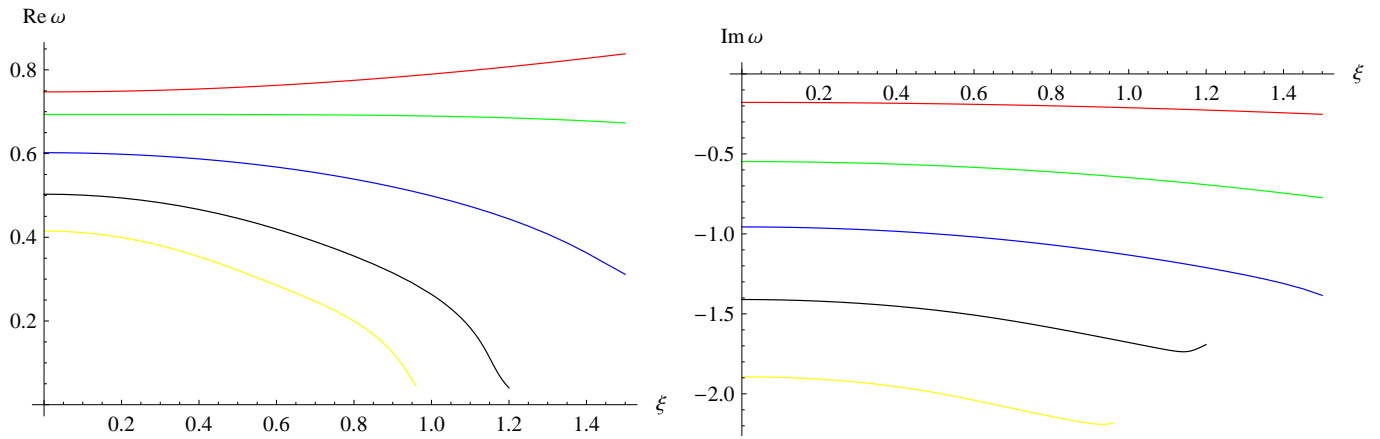


FIG. 9. The fundamental mode and the first four overtones as a function of ξ for the first black-hole model; $\ell = 2$ axial gravitational perturbations.

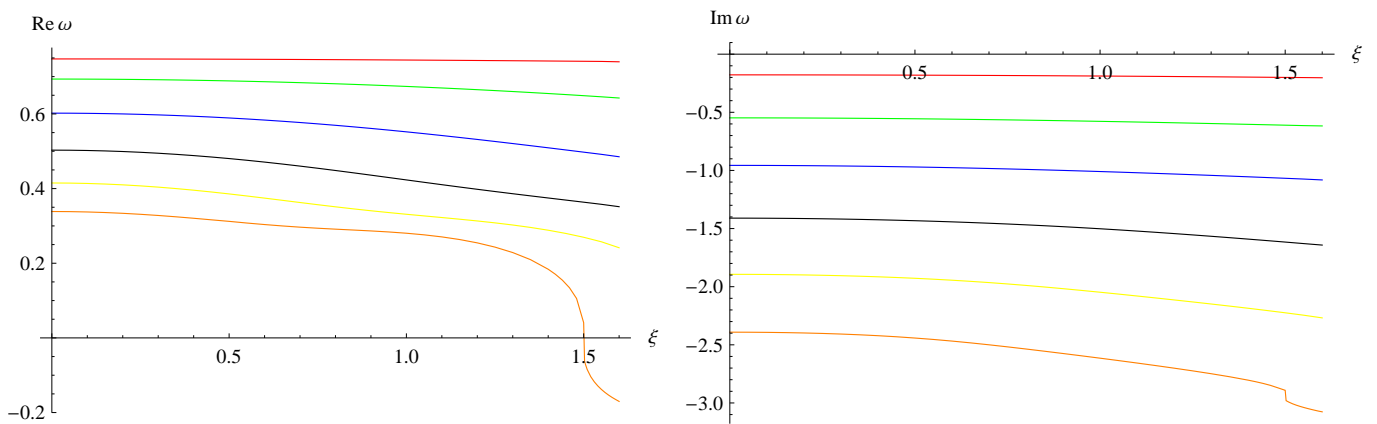


FIG. 10. The fundamental mode and the first five overtones as a function of ξ for the second black hole model; $\ell = 2$ axial gravitational perturbations.

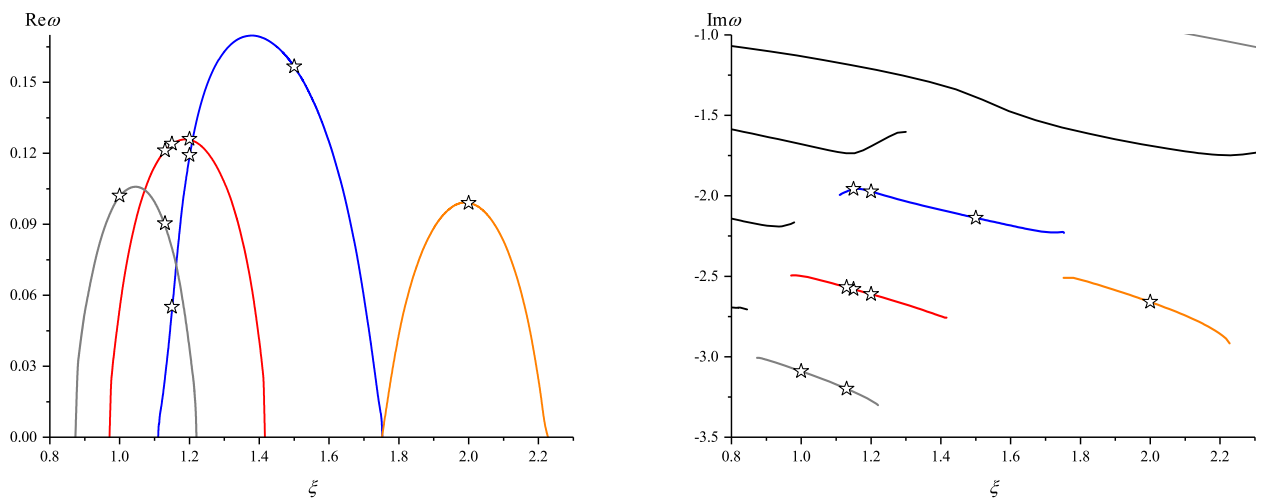


FIG. 11. The first non-perturbative modes as a function of ξ for the first black hole model; $\ell = 2$ axial gravitational perturbations. The star symbols correspond to the values from the Table IX

ξ	Prony fit	WKB6 Padé	Frobenius
0	0.218387 - 0.209629i	0.221584 - 0.209367i	0.220910 - 0.209791i
0.2	0.218610 - 0.211268i	0.221098 - 0.211264i	0.221198 - 0.211371i
0.4	0.219275 - 0.216279i	0.219706 - 0.215676i	0.222049 - 0.216145i
0.6	0.220437 - 0.224933i	0.221115 - 0.224992i	0.223427 - 0.224215i
0.8	0.222389 - 0.237582i	0.226484 - 0.243023i	0.225296 - 0.235748i
1.	0.225775 - 0.254226i	0.254696 - 0.241289i	0.227645 - 0.250970i
1.2	0.230904 - 0.274022i	0.235955 - 0.250742i	0.230537 - 0.270125i
1.4	0.236851 - 0.296233i	0.234166 - 0.275977i	0.234136 - 0.293402i

TABLE I. Comparison of the scalar ($s = 0$) quasinormal frequencies for the first BH model obtained by the time-domain integration and the 6th order WKB approach with Padé approximants and the Frobenius method for $\ell = 0$ ($M = 1/2$).

ξ	Prony fit	WKB6 Padé	rel. diff $Re(\omega)$	rel. diff $Im(\omega)$
0	0.585884 - 0.195294i	0.585859 - 0.195325i	0.00433%	0.0160%
0.2	0.587292 - 0.196837i	0.587283 - 0.196879i	0.00151%	0.0215%
0.4	0.591486 - 0.201473i	0.591499 - 0.201498i	0.00228%	0.0128%
0.6	0.598390 - 0.209219i	0.598435 - 0.209223i	0.00759%	0.00208%
0.8	0.607881 - 0.220103i	0.607916 - 0.220096i	0.00578%	0.00340%
1.	0.619800 - 0.234158i	0.619845 - 0.234331i	0.00733%	0.0737%
1.2	0.633960 - 0.251424i	0.633937 - 0.251460i	0.00355%	0.0143%
1.4	0.650159 - 0.271950i	0.650062 - 0.272029i	0.0150%	0.0291%

TABLE II. Comparison of the scalar ($s = 0$) quasinormal frequencies for the first BH model obtained by the time-domain integration and the 6th order WKB approach with Padé approximants $\ell = 1$ ($M = 1/2$).

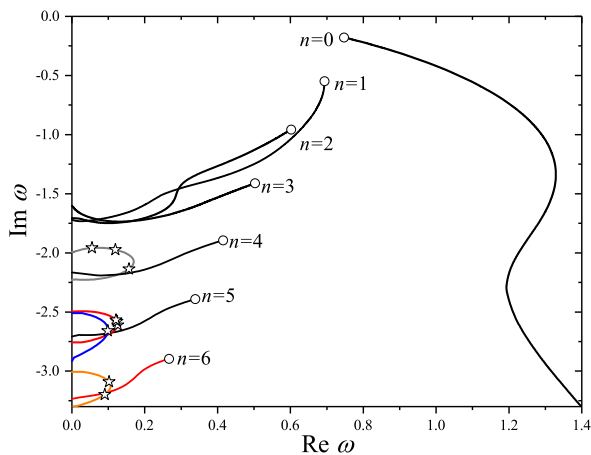


FIG. 12. The complex ω plane of QNMs. : The black lines represent the perturbative branches, while the colored lines correspond to the non-perturbative branches for the first black hole model; $\ell = 2$ axial gravitational perturbations.

frequencies (see, for example, fig. 12) that do not transition to the Schwarzschild frequencies. These modes may become purely imaginary, i.e., non-oscillatory, at certain values of ξ . Being non-perturbative in ξ , these modes cannot definitively be attributed to the quantum-corrected black hole, as the metric for the latter is constructed perturbatively in ξ .

Following the general procedure outlined in [63], we can derive an exact analytical formula for the quasinor-

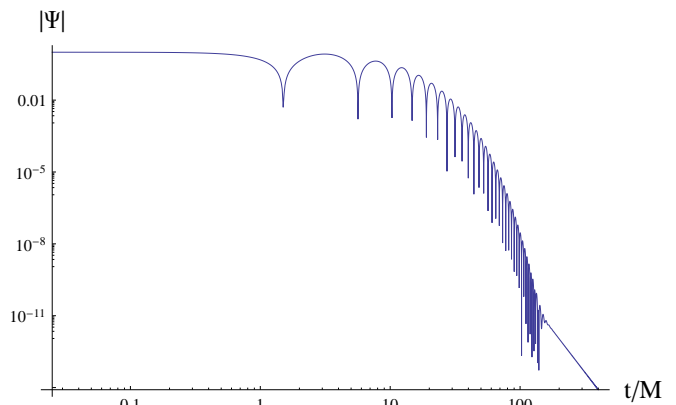


FIG. 13. Time-domain profile for axial gravitational perturbations of the first black hole model, $\ell = 2$, $M = 1/2$, $\xi = 0.3$.

mal frequencies in the eikonal limit, $\ell \gg n$. By expanding in powers of the inverse quantity $\kappa = \ell + 1/2$, we locate the position of the maximum of the effective potential. Remarkably, for both the first and second black hole models, this position coincides with that of the Schwarzschild case:

$$r_{max} = 3M + O\left(\frac{1}{\kappa}\right). \quad (32)$$

Then, using the first order WKB formula and the above expression for r_{max} we can find the frequencies in the form of expansion in terms of powers of ξ ;

ξ	Prony fit	WKB6 Padé	Frobenius
0	0.496524 - 0.184939i	0.496509 - 0.184993i	0.496527 - 0.184975i
0.2	0.497298 - 0.186108i	0.497313 - 0.186159i	0.497300 - 0.186143i
0.4	0.499584 - 0.189603i	0.499662 - 0.189645i	0.499586 - 0.189633i
0.6	0.503286 - 0.195384i	0.503416 - 0.195413i	0.503285 - 0.195407i
0.8	0.508246 - 0.203385i	0.508395 - 0.203405i	0.508242 - 0.203402i
1.	0.514264 - 0.213517i	0.514395 - 0.213536i	0.514255 - 0.213530i
1.2	0.521106 - 0.225669i	0.521194 - 0.225712i	0.521091 - 0.225683i
1.4	0.528519 - 0.239711i	0.528569 - 0.239834i	0.528498 - 0.239730i

TABLE III. Comparison of the electromagnetic ($s = 1$) quasinormal frequencies for the first black hole model obtained by the time-domain integration and the 6th order WKB approach with Padé approximants and Frobenius method for $\ell = 1$ ($M = 1/2$).

ξ	Prony fit	WKB6 Padé	Frobenius
0	0.218387 - 0.209629i	0.221584 - 0.209367i	0.220910 - 0.209791i
0.2	0.218499 - 0.210446i	0.221485 - 0.210223i	0.221054 - 0.210580i
0.4	0.218834 - 0.212908i	0.219813 - 0.212868i	0.221486 - 0.212943i
0.6	0.219402 - 0.217052i	0.219874 - 0.216627i	0.222202 - 0.216876i
0.8	0.220242 - 0.222932i	0.221167 - 0.223578i	0.223198 - 0.222368i
1.	0.221461 - 0.230599i	0.225523 - 0.235366i	0.224481 - 0.229407i
1.2	0.223260 - 0.240035i	0.248042 - 0.240253i	0.226069 - 0.237973i
1.4	0.225892 - 0.251044i	0.237632 - 0.229887i	0.227999 - 0.248035i

TABLE IV. Comparison of the quasinormal frequencies for the second BH model obtained by the time-domain integration and the 6th order WKB approach with Padé approximants for $s = 0$, $\ell = 0$ ($M = 1/2$).

$$\omega_n = \frac{\kappa}{3\sqrt{3}M} - \frac{i(2n+1)}{6\sqrt{3}M} + \xi^2 \left(\frac{\kappa}{162\sqrt{3}M^3} - \frac{i(2n+1)}{108\sqrt{3}M^3} \right) + \xi^4 \left(-\frac{\kappa}{17496\sqrt{3}M^5} + \frac{i(2n+1)}{34992\sqrt{3}M^5} \right) + O\left(\xi^5, \frac{1}{\kappa}\right). \quad (33)$$

In a similar way for the second black hole model, we have

$$\omega_n = \frac{\kappa}{3\sqrt{3}M} - \frac{i(2n+1)}{6\sqrt{3}M} - \xi^2 \frac{i(2n+1)}{324\sqrt{3}M^3} + \xi^4 \frac{i(2n+1)}{34992\sqrt{3}M^5} + O\left(\xi^5, \frac{1}{\kappa}\right). \quad (34)$$

When $\xi = 0$, the above formulas reduce to the well-known expressions for the Schwarzschild black hole [64].

It is worth mentioning that the above eikonal expressions for quasinormal modes are related to the parameters of the unstable null geodesics, such as the rotational frequency and Lyapunov exponent, via the correspondence established in [65]. However, there are a number of counterexamples to this correspondence [66–68]. In [69, 70] it was shown that the correspondence works only when the WKB approach can be applied and only to the part of the eikonal spectrum which can be found by the WKB method. Here we see that the correspondence takes place for both black hole models.

Within the recently discussed link between grey-body factors and amplitude of gravitational waves [71], a correspondence between the grey-body factors and quasinormal modes has been established [72]:

$$\Gamma_\ell(\omega) = \left(1 + e^{2\pi \frac{\omega^2 - \text{Re}(\omega_0)^2}{4\text{Re}(\omega_0)\text{Im}(\omega_0)}} \right)^{-1} + \Sigma(\omega_0, \omega_1). \quad (35)$$

Here $\Sigma(\omega_0, \omega_1)$ is the sum of the correction terms beyond the eikonal limit found in [72].

This relation, which connects the grey-body factors $\Gamma_\ell(\omega)$ with the fundamental quasinormal mode ω_0 , is exact in the eikonal limit as $\ell \rightarrow \infty$. By introducing corrections involving the first overtone ω_1 , this relation also provides an approximate correspondence for lower ℓ . Consequently, the quasinormal modes obtained here can be used to determine the grey-body factors. In the eikonal regime, the grey-body factors can be immediately derived analytically using the eikonal expressions (33) and (34) for the quasinormal modes ω_1 and ω_2 in (35).

It is worth mentioning that, at asymptotically late times, the quasinormal ringing transitions to power-law tails, which are indistinguishable from the Price law for the Schwarzschild solution [73] (see fig. 13),

$$|\Psi| \sim t^{-(2\ell+3)}, \quad t \rightarrow \infty. \quad (36)$$

ξ	Prony fit	WKB6 Padé	rel. diff $Re(\omega)$	rel. diff $Im(\omega)$
0	0.585884 - 0.195294 <i>i</i>	0.585859 - 0.195325 <i>i</i>	0.00433%	0.0160%
0.2	0.585931 - 0.195908 <i>i</i>	0.585917 - 0.195954 <i>i</i>	0.00227%	0.0233%
0.4	0.586068 - 0.197743 <i>i</i>	0.586066 - 0.197780 <i>i</i>	0.00033%	0.0185%
0.6	0.586294 - 0.200778 <i>i</i>	0.586314 - 0.200800 <i>i</i>	0.00342%	0.0109%
0.8	0.586605 - 0.204978 <i>i</i>	0.586647 - 0.204985 <i>i</i>	0.00716%	0.00333%
1.	0.586997 - 0.210299 <i>i</i>	0.587029 - 0.210295 <i>i</i>	0.00542%	0.00186%
1.2	0.587463 - 0.216690 <i>i</i>	0.587328 - 0.216803 <i>i</i>	0.0230%	0.0519%
1.4	0.588000 - 0.224098 <i>i</i>	0.588225 - 0.224214 <i>i</i>	0.0383%	0.0516%

TABLE V. Comparison of the quasinormal frequencies for the second BH model obtained by the time-domain integration and the 6th order WKB approach with Padé approximants for $s = 0$, $\ell = 1$ ($M = 1/2$).

ξ	Prony fit	WKB6 Padé	rel. diff $Re(\omega)$	rel. diff $Im(\omega)$
0	0.496524 - 0.184939 <i>i</i>	0.496509 - 0.184993 <i>i</i>	0.00310%	0.0295%
0.2	0.496186 - 0.185294 <i>i</i>	0.496183 - 0.185348 <i>i</i>	0.00066%	0.0289%
0.4	0.495174 - 0.186348 <i>i</i>	0.495205 - 0.186400 <i>i</i>	0.00620%	0.0281%
0.6	0.493501 - 0.188066 <i>i</i>	0.493583 - 0.188122 <i>i</i>	0.0166%	0.0299%
0.8	0.491187 - 0.190398 <i>i</i>	0.491330 - 0.190469 <i>i</i>	0.0291%	0.0376%
1.	0.488257 - 0.193274 <i>i</i>	0.488464 - 0.193380 <i>i</i>	0.0424%	0.0545%
1.2	0.484743 - 0.196619 <i>i</i>	0.485010 - 0.196784 <i>i</i>	0.0551%	0.0838%
1.4	0.480680 - 0.200350 <i>i</i>	0.480996 - 0.200607 <i>i</i>	0.0657%	0.128%

TABLE VI. Comparison of the quasinormal frequencies for the second BH model obtained by the time-domain integration and the 6th order WKB approach with Padé approximants for $s = 1$, $\ell = 1$ ($M = 1/2$).

V. BLACK HOLE SHADOWS

The fundamental equations for calculating the radius of a black hole shadow have been known for a long time [74, 75] and have been applied in numerous studies (see, for example, [76–82] and references therein).

The radius of the circular photon orbit r_{ph} of static, spherically-symmetric spacetime can be defined as the solution of the following equation [74–77]

$$rf'(r) - 2f(r) = 0. \quad (37)$$

Then the shadow radius R_{sh} of the photon sphere r_{ph} observed by the distant observer is given by [74, 83]

$$R_{\text{sh}} = \frac{r_{\text{ph}}}{\sqrt{f(r_{\text{ph}})}}. \quad (38)$$

For the first model, we have

$$(r - 3M)(4M\xi^2 - r^3 - 2\xi^2 r) = 0, \quad (39)$$

which yields

$$r_{\text{ph}} = 3M, \quad R_{\text{sh}} = \frac{27M^2}{\sqrt{\xi^2 + 27M^2}}. \quad (40)$$

For the second model, we have

$$r_{\text{ph}} = 3M, \quad R_{\text{sh}} = 3\sqrt{3}M, \quad (41)$$

which coincides with the case of the Schwarzschild black hole.

We can use the recent results of the EHT observations of the black hole shadow to restrict the value of the quantum parameter ξ .

From observations of the shadow cast by Sgr A* black hole [18, 84], we have [85]

$$4.55M \lesssim R_{\text{sh}} \lesssim 5.22M, \quad (1\sigma). \quad (42)$$

This provides the following range for ξ for the first model

$$0 \leq \xi \lesssim 2.866M. \quad (43)$$

For the second model, ξ cannot be restricted through the current black hole shadow observations

$$0 \leq \xi < \infty. \quad (44)$$

VI. CONCLUSIONS

While quasinormal modes of various models of quantum-corrected black holes have been extensively studied in recent years, no such studies have been conducted for the two recently proposed black hole models developed using the Hamiltonian constraints approach, which preserves general covariance [1].

In this work, we have demonstrated that the quasinormal modes for the two models of quantum-corrected black holes differ significantly from each other and from their classical (Schwarzschild) counterparts. However, there is a common feature for both models: while the fundamental mode changes slowly as the quantum parameter increases, the first few overtones deviate at an

ξ	Prony fit	WKB6 Padé	Frobenius
0	0.747356 - 0.177914 <i>i</i>	0.747238 - 0.177857 <i>i</i>	0.747343 - 0.177925 <i>i</i>
0.2	0.749129 - 0.179257 <i>i</i>	0.749131 - 0.179207 <i>i</i>	0.749116 - 0.179267 <i>i</i>
0.4	0.754411 - 0.183281 <i>i</i>	0.754477 - 0.183222 <i>i</i>	0.754397 - 0.183291 <i>i</i>
0.6	0.763091 - 0.189975 <i>i</i>	0.763323 - 0.189879 <i>i</i>	0.763076 - 0.189986 <i>i</i>
0.8	0.774994 - 0.199321 <i>i</i>	0.775636 - 0.199279 <i>i</i>	0.774977 - 0.199333 <i>i</i>
1.	0.789893 - 0.211295 <i>i</i>	0.791334 - 0.211781 <i>i</i>	0.789874 - 0.211309 <i>i</i>
1.2	0.807521 - 0.225870 <i>i</i>	0.809481 - 0.227926 <i>i</i>	0.807499 - 0.225885 <i>i</i>
1.4	0.827586 - 0.243013 <i>i</i>	0.828953 - 0.246556 <i>i</i>	0.827562 - 0.243031 <i>i</i>
1.6	0.849785 - 0.262694 <i>i</i>	0.850556 - 0.266906 <i>i</i>	0.849757 - 0.262714 <i>i</i>

TABLE VII. Comparison of the quasinormal frequencies for axial gravitational perturbations ($s = 2$) of the first black hole model obtained by the time-domain integration and the 6th order WKB approach with Padé approximants; $\ell = 2$, $M = 1/2$.

ξ	Prony fit	WKB6 Padé	Frobenius
0	0.747356 - 0.177914 <i>i</i>	0.747238 - 0.177857 <i>i</i>	0.747343 - 0.177925 <i>i</i>
0.2	0.747233 - 0.178332 <i>i</i>	0.747223 - 0.178282 <i>i</i>	0.747220 - 0.178342 <i>i</i>
0.4	0.746867 - 0.179577 <i>i</i>	0.746903 - 0.179548 <i>i</i>	0.746854 - 0.179587 <i>i</i>
0.6	0.746267 - 0.181630 <i>i</i>	0.746416 - 0.181571 <i>i</i>	0.746253 - 0.181640 <i>i</i>
0.8	0.745445 - 0.184461 <i>i</i>	0.745869 - 0.184430 <i>i</i>	0.745431 - 0.184471 <i>i</i>
1.	0.744418 - 0.188031 <i>i</i>	0.745422 - 0.188359 <i>i</i>	0.744404 - 0.188042 <i>i</i>
1.2	0.743204 - 0.192298 <i>i</i>	0.744773 - 0.194024 <i>i</i>	0.743190 - 0.192309 <i>i</i>
1.4	0.741820 - 0.197217 <i>i</i>	0.742607 - 0.200808 <i>i</i>	0.741805 - 0.197228 <i>i</i>
1.6	0.740283 - 0.202745 <i>i</i>	0.739969 - 0.207172 <i>i</i>	0.740267 - 0.202756 <i>i</i>

TABLE VIII. Comparison of the quasinormal frequencies for axial gravitational perturbations ($s = 2$) of the second BH model obtained by the time-domain integration and the 6th order WKB approach with Padé approximants: $\ell = 2$, $M = 1/2$.

increasing rate from their Schwarzschild values, creating a characteristic "sound" of the event horizon. The real oscillation frequencies of the overtones rapidly approach zero as the quantum correction intensifies. The three independent methods used to find quasinormal modes—WKB approach, time-domain integration, and Frobenius method—are in very good agreement within the common range of their applicability. In the high-frequency (eikonal) regime, analytic formulas for quasinormal modes have been derived. In addition to studying the branch of modes that are perturbative in the quantum parameter ξ , we observed frequencies that are non-perturbative in this parameter and exist at intermediate values of ξ . This non-perturbative branch of modes warrants more detailed study, especially if they are observed at sufficiently small values of ξ .

We have also calculated the radius of the shadow cast by both black hole models and demonstrated that, while the parameter ξ in the first model could be constrained by observations of the Sgr A* black hole, the second model has a Schwarzschildian radius of shadows and does not allow for such a constraint.

Our work could be extended in several directions. While we focused on the most interesting bosonic perturbations, a similar analysis could be conducted for fermionic perturbations, particularly those describing neutrino perturbations. Additionally, the analytic formula derived in the eikonal limit could be extended to higher orders, providing a more accurate analytical approximation for the numerical data obtained in this

study.

ACKNOWLEDGMENTS

R. A. K. acknowledges A. Zhidenko for useful discussions. O.S. is grateful to the Page family for their kind hospitality in Princeton.

ξ	PS	Frobenius method	rel. diff. $Re(\omega)$	rel. diff. $Im(\omega)$
1	$0.102 - 3.0901i$	$0.102225 - 3.090315i$	0.157%	0.012%
1.13	$0.1212 - 2.5679i$	$0.121201 - 2.567954i$	0.0095%	0.0025%
	$0.0904 - 3.1989i$	$0.08986 - 3.19839i$	0.562%	0.017%
1.15	$0.05503 - 1.9585i$	$0.053611 - 1.9592i$	2.65%	0.0384%
	$0.124 - 2.5799i$	$0.124053 - 2.579967i$	0.0378%	0.001%
1.2	$0.11921 - 1.973i$	$0.119201 - 1.973059i$	0.0048%	0.001%
	$0.126 - 2.6106i$	$0.125993 - 2.61059i$	0.011%	0.0019%
2	$0.0989 - 2.6595i$	$0.099091 - 2.659618i$	0.1711%	0.0037%

TABLE IX. Comparison of the nonperturbative quasinormal frequencies for axial gravitational perturbations ($s = 2$) of the first BH model obtained by the pseudospectral (PS) method and by the Frobenius method: $\ell = 2$, $M = 1/2$.

-
- [1] Cong Zhang, Jerzy Lewandowski, Yongge Ma, and Jinsong Yang. Black Holes and Covariance in Effective Quantum Gravity, arXiv: 2407.10168. 7 2024.
- [2] Abhay Ashtekar, Martin Bojowald, and Jerzy Lewandowski. Mathematical structure of loop quantum cosmology. *Adv. Theor. Math. Phys.*, 7:233–268, 2003.
- [3] Andrew Strominger and Cumrun Vafa. Microscopic origin of the Bekenstein-Hawking entropy. *Phys. Lett. B*, 379:99–104, 1996.
- [4] John F. Donoghue. General relativity as an effective field theory: The leading quantum corrections. *Phys. Rev. D*, 50:3874–3888, 1994.
- [5] Piero Nicolini, Anais Smailagic, and Euro Spallucci. Non-commutative geometry inspired Schwarzschild black hole. *Phys. Lett. B*, 632:547–551, 2006.
- [6] Juan Martin Maldacena. The Large N limit of superconformal field theories and supergravity. *Int. J. Theor. Phys.*, 38:1113–1133, 1999.
- [7] Max Niedermaier and Martin Reuter. The Asymptotic Safety Scenario in Quantum Gravity. *Living Rev. Rel.*, 9:5, 2006.
- [8] Thomas Thiemann. *Modern Canonical Quantum General Relativity*. Cambridge University Press, Cambridge, UK, 2007.
- [9] Abhay Ashtekar and Jerzy Lewandowski. Background independent quantum gravity: A status report. *Class. Quant. Grav.*, 21:R53, 2004.
- [10] Kostas D. Kokkotas and Bernd G. Schmidt. Quasinormal modes of stars and black holes. *Living Rev. Rel.*, 2:2, 1999.
- [11] R. A. Konoplya and A. Zhidenko. Quasinormal modes of black holes: From astrophysics to string theory. *Rev. Mod. Phys.*, 83:793–836, 2011.
- [12] B. P. Abbott et al. GW170817: Observation of Gravitational Waves from a Binary Neutron Star Inspiral. *Phys. Rev. Lett.*, 119(16):161101, 2017.
- [13] R. Abbott et al. GW190814: Gravitational Waves from the Coalescence of a 23 Solar Mass Black Hole with a 2.6 Solar Mass Compact Object. *Astrophys. J. Lett.*, 896(2):L44, 2020.
- [14] K. G. Arun et al. New horizons for fundamental physics with LISA. *Living Rev. Rel.*, 25(1):4, 2022.
- [15] R. A. Konoplya. The sound of the event horizon. *Int. J. Mod. Phys. D*, 32(14):2342014, 2023.
- [16] R. A. Konoplya and A. Zhidenko. First few overtones probe the event horizon geometry, arXiv: 2209.00679. 9 2022.
- [17] Matthew Giesler, Maximiliano Isi, Mark A. Scheel, and Saul Teukolsky. Black Hole Ringdown: The Importance of Overtones. *Phys. Rev. X*, 9(4):041060, 2019.
- [18] Kazunori Akiyama et al. First M87 Event Horizon Telescope Results. I. The Shadow of the Supermassive Black Hole. *Astrophys. J. Lett.*, 875:L1, 2019.
- [19] Cosimo Bambi. Testing black hole candidates with electromagnetic radiation. *Rev. Mod. Phys.*, 89(2):025001, 2017.
- [20] S. V. Bolokhov. Long-lived quasinormal modes and overtones’ behavior of holonomy-corrected black holes. *Phys. Rev. D*, 110(2):024010, 2024.
- [21] S. V. Bolokhov. Long-lived quasinormal modes and oscillatory tails of the Bardeen spacetime. *Phys. Rev. D*, 109(6):064017, 2024.
- [22] Milena Skvortsova. Quasinormal Frequencies of Fields with Various Spin in the Quantum Oppenheimer-Snyder Model of Black Holes, arXiv: 2405.06390. 5 2024.
- [23] Alexey Dubinsky. Quantum gravitational corrections to the Schwarzschild spacetime and quasinormal frequencies, arXiv: 2405.13552. 5 2024.
- [24] Alexey Dubinsky. Quasinormal modes of charged black holes in Asymptotically Safe Gravity, arXiv: 2405.08262. 5 2024.
- [25] S. V. Bolokhov, K. A. Bronnikov, and R. A. Konoplya. Can quantum gravity effects accelerate black hole evaporation?, arXiv: 2306.11083. 6 2023.
- [26] R. A. Konoplya. Quantum corrected black holes: quasinormal modes, scattering, shadows. *Phys. Lett. B*, 804:135363, 2020.
- [27] R. A. Konoplya, D. Ovchinnikov, and B. Ahmedov. Bardeen spacetime as a quantum corrected Schwarzschild black hole: Quasinormal modes and Hawking radiation. *Phys. Rev. D*, 108(10):104054, 2023.
- [28] Huajie Gong, Shulan Li, Dan Zhang, Guoyang Fu, and Jian-Pin Wu. Quasinormal modes of quantum-corrected black holes, arXiv: 2312.17639. 12 2023.
- [29] M. B. Cruz, F. A. Brito, and C. A. S. Silva. Polar gravitational perturbations and quasinormal modes of a loop quantum gravity black hole. *Phys. Rev. D*, 102(4):044063, 2020.
- [30] Ramin G. Daghigh, Michael D. Green, and Gabor Kunstatter. Scalar Perturbations and Stability of a Loop Quantum Corrected Kruskal Black Hole. *Phys. Rev. D*, 103(8):084031, 2021.

- [31] Oleksandr Stashko. Quasinormal modes and gray-body factors of regular black holes in asymptotically safe gravity. *arXiv e-prints*, page arXiv:2407.07892, July 2024.
- [32] Chao Zhang and Anzhong Wang. Quasi-Normal Modes of Loop Quantum Black Holes Formed from Gravitational Collapse. *arXiv e-prints*, page arXiv:2407.19654, July 2024.
- [33] Emanuele Berti, Vitor Cardoso, and Andrei O. Starinets. Quasinormal modes of black holes and black branes. *Class. Quant. Grav.*, 26:163001, 2009.
- [34] Abhay Ashtekar, Javier Olmedo, and Parampreet Singh. Quantum Transfiguration of Kruskal Black Holes. *Phys. Rev. Lett.*, 121(24):241301, 2018.
- [35] Abhay Ashtekar, Javier Olmedo, and Parampreet Singh. Quantum extension of the Kruskal spacetime. *Phys. Rev. D*, 98(12):126003, 2018.
- [36] Mariam Bouhmadi-López, Suddhasattwa Brahma, Che-Yu Chen, Pisin Chen, and Dong-han Yeom. A consistent model of non-singular Schwarzschild black hole in loop quantum gravity and its quasinormal modes. *JCAP*, 07:066, 2020.
- [37] Emanuele Berti, Kostas D. Kokkotas, and Eleftherios Papantonopoulos. Gravitational stability of five-dimensional rotating black holes projected on the brane. *Phys. Rev. D*, 68:064020, 2003.
- [38] K. D. Kokkotas. Quasinormal modes of the Kerr-Newman black hole. *Nuovo Cim. B*, 108:991–998, 1993.
- [39] R. A. Konoplya and A. Zhidenko. Gravitational spectrum of black holes in the Einstein-Aether theory. *Phys. Lett. B*, 648:236–239, 2007.
- [40] Tullio Regge and John A. Wheeler. Stability of a Schwarzschild singularity. *Phys. Rev.*, 108:1063–1069, 1957.
- [41] K. A. Bronnikov, R. A. Konoplya, and A. Zhidenko. Instabilities of wormholes and regular black holes supported by a phantom scalar field. *Phys. Rev. D*, 86:024028, 2012.
- [42] Che-Yu Chen and Pisin Chen. Gravitational perturbations of nonsingular black holes in conformal gravity. *Phys. Rev. D*, 99(10):104003, 2019.
- [43] R. A. Konoplya, A. Zhidenko, and A. F. Zinhailo. Higher order WKB formula for quasinormal modes and grey-body factors: recipes for quick and accurate calculations. *Class. Quant. Grav.*, 36:155002, 2019.
- [44] Sai Iyer and Clifford M. Will. Black Hole Normal Modes: A WKB Approach. 1. Foundations and Application of a Higher Order WKB Analysis of Potential Barrier Scattering. *Phys. Rev. D*, 35:3621, 1987.
- [45] R. A. Konoplya. Quasinormal behavior of the d-dimensional Schwarzschild black hole and higher order WKB approach. *Phys. Rev. D*, 68:024018, 2003.
- [46] R. A. Konoplya. Quasinormal modes of the Schwarzschild black hole and higher order WKB approach. *J. Phys. Stud.*, 8:93–100, 2004.
- [47] Jerzy Matyjasek and Michał Opala. Quasinormal modes of black holes. The improved semianalytic approach. *Phys. Rev. D*, 96(2):024011, 2017.
- [48] Carsten Gundlach, Richard H. Price, and Jorge Pullin. Late time behavior of stellar collapse and explosions: 1. Linearized perturbations. *Phys. Rev. D*, 49:883–889, 1994.
- [49] E. W. Leaver. An Analytic representation for the quasinormal modes of Kerr black holes. *Proc. Roy. Soc. Lond. A*, 402:285–298, 1985.
- [50] Edward W. Leaver. Spectral decomposition of the perturbation response of the Schwarzschild geometry. *Phys. Rev. D*, 34:384–408, 1986.
- [51] Hans-Peter Nollert. Quasinormal modes of Schwarzschild black holes: The determination of quasinormal frequencies with very large imaginary parts. *Phys. Rev. D*, 47:5253–5258, 1993.
- [52] Alexander Zhidenko. Massive scalar field quasi-normal modes of higher dimensional black holes. *Phys. Rev. D*, 74:064017, 2006.
- [53] Andrzej Rostworowski. Quasinormal frequencies of D-dimensional Schwarzschild black holes: Evaluation via continued fraction method. *Acta Phys. Polon. B*, 38:81–89, 2007.
- [54] J.P. Boyd. *Chebyshev and Fourier Spectral Methods: Second Revised Edition*. Dover Books on Mathematics. Dover Publications, 2013.
- [55] A. F. Zinhailo. Black Hole in the Quantum Oppenheimer-Snyder model: long lived modes and the overtones’ behavior, Research Gate preprint doi: 10.13140/RG.2.2.26785.01124. 2024.
- [56] Antonina F. Zinhailo. Exploring unique quasinormal modes of a massive scalar field in brane-world scenarios. *Phys. Lett. B*, 853:138682, 2024.
- [57] R. A. Konoplya. Massive vector field perturbations in the Schwarzschild background: Stability and unusual quasinormal spectrum. *Phys. Rev. D*, 73:024009, 2006.
- [58] R. A. Konoplya, A. F. Zinhailo, J. Kunz, Z. Stuchlik, and A. Zhidenko. Quasinormal ringing of regular black holes in asymptotically safe gravity: the importance of overtones. *JCAP*, 10:091, 2022.
- [59] R. A. Konoplya. Quasinormal modes in higher-derivative gravity: Testing the black hole parametrization and sensitivity of overtones. *Phys. Rev. D*, 107(6):064039, 2023.
- [60] R. A. Konoplya, Z. Stuchlik, A. Zhidenko, and A. F. Zinhailo. Quasinormal modes of renormalization group improved Dymnikova regular black holes. *Phys. Rev. D*, 107(10):104050, 2023.
- [61] R. A. Konoplya. Quasinormal modes and grey-body factors of regular black holes with a scalar hair from the Effective Field Theory. *JCAP*, 07:001, 2023.
- [62] Dan Zhang, Huajie Gong, Guoyang Fu, Jian-Pin Wu, and Qiyuan Pan. Quasinormal modes of a regular black hole with sub-Planckian curvature. *Eur. Phys. J. C*, 84(6):564, 2024.
- [63] R. A. Konoplya and A. Zhidenko. Analytic expressions for quasinormal modes and grey-body factors in the eikonal limit and beyond. *Class. Quant. Grav.*, 40(24):245005, 2023.
- [64] Hans-Joachim Blome and Bahram Mashhoon. Quasinormal oscillations of a schwarzschild black hole. *Phys. Lett. A*, 100(5):231–234, 1981.
- [65] Vitor Cardoso, Alex S. Miranda, Emanuele Berti, Helvi Wittek, and Wilson T. Zanchin. Geodesic stability, Lyapunov exponents and quasinormal modes. *Phys. Rev. D*, 79(6):064016, 2009.
- [66] R. A. Konoplya, A. F. Zinhailo, and Z. Stuchlik. Quasinormal modes, scattering, and Hawking radiation in the vicinity of an Einstein-dilaton-Gauss-Bonnet black hole. *Phys. Rev. D*, 99(12):124042, 2019.
- [67] R. A. Konoplya and A. F. Zinhailo. Quasinormal modes, stability and shadows of a black hole in the 4D Einstein-Gauss-Bonnet gravity. *Eur. Phys. J. C*, 80(11):1049, 2020.

- [68] S. V. Bolokhov. Black holes in Starobinsky-Bel-Robinson Gravity and the breakdown of quasinormal modes/null geodesics correspondence. *Phys. Lett. B*, 856:138879, 2024.
- [69] R. A. Konoplya and Z. Stuchlík. Are eikonal quasinormal modes linked to the unstable circular null geodesics? *Phys. Lett. B*, 771:597–602, 2017.
- [70] R. A. Konoplya. Further clarification on quasinormal modes/circular null geodesics correspondence. *Phys. Lett. B*, 838:137674, 2023.
- [71] Naritaka Oshita. Greybody factors imprinted on black hole ringdowns: An alternative to superposed quasinormal modes. *Phys. Rev. D*, 109(10):104028, 2024.
- [72] R. A. Konoplya and A. Zhidenko. Correspondence between grey-body factors and quasinormal modes, arXiv: 2406.11694. 6 2024.
- [73] Richard H. Price. Nonspherical perturbations of relativistic gravitational collapse. 1. Scalar and gravitational perturbations. *Phys. Rev. D*, 5:2419–2438, 1972.
- [74] J. L. Synge. The Escape of Photons from Gravitationally Intense Stars. *Mon. Not. Roy. Astron. Soc.*, 131(3):463–466, 1966.
- [75] Clarissa-Marie Claudel, K. S. Virbhadra, and G. F. R. Ellis. The geometry of photon surfaces. *Journal of Mathematical Physics*, 42(2):818–838, February 2001.
- [76] K. S. Virbhadra and G. F. R. Ellis. Gravitational lensing by naked singularities. *Phys. Rev. D*, 65:103004, 2002.
- [77] Volker Perlick and Oleg Yu. Tsupko. Calculating black hole shadows: Review of analytical studies. *Phys. Rept.*, 947:1–39, 2022.
- [78] Gennady S. Bisnovatyi-Kogan and Oleg Yu. Tsupko. Gravitational Lensing in Presence of Plasma: Strong Lens Systems, Black Hole Lensing and Shadow. *Universe*, 3(3):57, 2017.
- [79] Volker Perlick, Oleg Yu. Tsupko, and Gennady S. Bisnovatyi-Kogan. Influence of a plasma on the shadow of a spherically symmetric black hole. *Phys. Rev. D*, 92(10):104031, 2015.
- [80] R. A. Konoplya. Shadow of a black hole surrounded by dark matter. *Phys. Lett. B*, 795:1–6, 2019.
- [81] Qingyu Gan, Peng Wang, Houwen Wu, and Haitang Yang. Photon ring and observational appearance of a hairy black hole. *Phys. Rev. D*, 104(4):044049, 2021.
- [82] Cheng Liu, Tao Zhu, Qiang Wu, Kimet Jusufi, Mubasher Jamil, Mustapha Azreg-Aïnou, and Anzhong Wang. Shadow and quasinormal modes of a rotating loop quantum black hole. *Phys. Rev. D*, 101(8):084001, 2020. [Erratum: *Phys.Rev.D* 103, 089902 (2021)].
- [83] Psaltis et al. Gravitational test beyond the first post-newtonian order with the shadow of the m87 black hole. *Phys. Rev. Lett.*, 125:141104, Oct 2020.
- [84] Kazunori Akiyama et al. First M87 Event Horizon Telescope Results. VI. The Shadow and Mass of the Central Black Hole. *Astrophys. J. Lett.*, 875(1):L6, 2019.
- [85] Sunny Vagnozzi et al. Horizon-scale tests of gravity theories and fundamental physics from the event horizon telescope image of sagittarius a. *Classical and Quantum Gravity*, 40(16):165007, July 2023.